A numerical study of the environmental conditions in nanoscale air bearings affecting smear formation

Roshan Mathew Tom[1], David Bogy[1]

[1]Department of Mechanical Engineering, UC Berkeley, Berkeley, CA, 94720

Abstract

We use the direct simulation Monte Carlo (DSMC) method along with the consistent Boltzmann algorithm to study the environmental factors affecting smear formation in a representative HAMR air bearing. We focus on the humidity, temperature, density, and velocity fields occurring due to the high-temperature hotspot on the disk and head surfaces. The results suggest that the density and temperature fields remain generally the same through the gas channel due to the presence of the free molecular gas flow in the air-bearing. This is possible as the head-disk clearance limits the mean-free path of the various molecules. Further, we find that the high temperature increases the water vapor concentration as the peak pressure increases. We also recommend methods for further study on smear formation in the head-disk interface.

Index Terms

Heat-Assisted Magnetic Recording, Smear, Head-Disk Interface.

I. Introduction

HEAT-ASSISTED magnetic recording (HAMR) is the most promising technology to increase the areal density of hard disk drives [1]. This technology embeds a laser in the recording head that heats a nanoscale spot on the disk to several hundred degrees to write data before cooling down to freeze data at room temperature. The large temperature gradient, accompanied by the electric field gradient, however, can cause the premature failure of these heads. Therefore, it is critical to design a robust head-disk interface for the long-term success of HAMR. Several experiments conducted on the head-disk interface reveal the presence of contaminations on the head and disk surfaces [2, 3]. These contaminations appear smeared on the surfaces and are commonly called "smear." They are formed from several sources, such as the PFPE lubricant, disk materials, and air-borne contaminants like silica. An atomic-force microscopy image of smear is shown in Fig. 1. The air-bearing that supports the slider to maintain a steady head-disk spacing can be as low as 1 nm. Therefore, smear can cause significant instabilities in the sliders' flying characteristics, eventually leading to a crash on the disk. Mitigating smear is key in developing reliable HAMR drives and has seen considerable research attention [4–8].

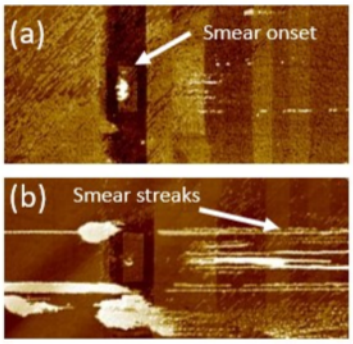

Fig. 1. AFM Image of smear from ref. [5]

A critical step in studying smear is to understand its formation and the factors that influence its growth. Several mechanisms have been proposed [4, 5, 9, 10]. The temperature gradient has seen the most attention, however, other forces such as optical forces has also been studied. Due to the multi-dimensional nature of smear, including its diverse composition, it is likely that multiple mechanisms act concurrently to influence the onset and growth of smear. The area where the smear grows - the head-disk interface - exceeds several microns in the down-track and cross-track directions but is only several nanometers in the vertical direction. This raises the important question of whether to model the surfaces and smear as a continuum solid/fluid

Corresponding author: R.M. Tom (email: roshantom@berkeley.edu).

or as atoms and molecules. Each assumption would have its own advantages and disadvantages. Nevertheless, they both have been used to extend our understanding of smear formation and mitigation [5, 11, 12]. Arguably, each model would inform the other to create a robust simulation strategy that can capture all facets of smear.

The minimum thickness of the air bearing can be as low as 1 nm, which is only three to four helium atoms wide. The modeling and design of the air-bearing, however, is primarily done using a thin-film continuum theory [13]. Nevertheless, a particle-based study showed that the continuum theory yields similar results when calculating the bearing forces on the slider [14]. However, the air-bearing in HAMR presents introduces new conditions - the temperature hotspot. Given that the primary medium of smear transport is the air-bearing, the characteristics of the air-bearing under this temperature field need to be investigated. In this report, we look into the temperature, density, and velocity fields in a representative HAMR gas bearing.

Humidity is also important to the reliability of HAMR. It has been shown to induce a water monolayer on the disk surface [15, 16], decrease the tribocharge in the slider-disk interface [17], influence the lubricant transfer between the head and the disk [18], enhance the heat transfer between the protrusions from the head in contact with the disk when the RH is greater than 75% [19], affect the spreading rate and chemisorption of the lubricants on the disk surface [20], reduce the vaporization energy and thus increase evaporation of lubricants during thermal desorption [21, 22], and promote corrosion of the recording layers [23]. These results show a clear relationship between humidity and the reliability of hard disk drives. Therefore, we also consider the behavior of water molecules in the air-bearing.

In Section II, we begin by describing the model used to simulate the air-bearing. We use a particle-based method, Direct Simulation Monte Carlo (DSMC), with a dense gas modification. Further, we explain the simulation conditions, specifically the approximation of the head-disk interface. We then present the results of our simulation in Section III. Finally, in Section IV, we present the conclusions and the scope for further study.

II. Numerical Model

A. Simulation method

The molecular gas lubrication (MGL) theory, along with the Fukui-Keneko method, is the accepted method to solve for the properties of the gas bearings in the head-disk interface [13]. However, it does not give insight into the molecular nature of the gas-bearing. Since the minimum head-disk clearance in recent hard drives is around 1 nm, the particle nature of the air-bearing can have a significant impact on the movement of contaminants in the head-disk interface. In this study, we use a particle-based method called Direct Simulation Monte Carlo (DSMC) to study the air bearings in HAMR head-disk interface conditions.

The DSMC method solves the Boltzmann Transport Equation by tracking the trajectory of individual particles (atoms and molecules) in the simulation domain [24]. Statistical averages are then taken to extract macroscopic properties. Unlike a molecular dynamics (MD) simulation, it employs the use of stochastic functions to calculate the collision, position, and velocity of the particles [25]. The method begins by using simulated particles that are statistical equivalents of real particles. If each real particle can be represented by its position and velocity, $\{\boldsymbol{x}, \boldsymbol{v}\}$, then all real particles within the space $\{\boldsymbol{x} + \mathrm{d}\boldsymbol{x}, \boldsymbol{v} + \mathrm{d}\boldsymbol{v}\}$ are represented by one simulated particle. The positions, velocities distribution, and collisions of the DSMC particle are chosen to match that of real particles. The ratio between the simulated and real particles is a global input to the solver. The initial velocity distribution is governed by the Maxwell-Boltzmann distribution given by,

$$f(\boldsymbol{v}) = \left[\frac{m}{2\pi k_B T}\right]^{3/2} \exp\left(-\frac{m\boldsymbol{v}^2}{2k_B T}\right) \tag{1}$$

where m, k_B, T, and v are the particle mass, the Boltzmann constant, the local temperature, and the particle velocity. At each timestep, the collision and movement of the particles are decoupled. First, each particle is advected along its velocity by Newtonian mechanics. Then, collisions between particles are calculated. In physical fluids, two particles that are separated by a distance greater than their mean free path rarely collide. Therefore, DSMC divides the domain into discrete cells that are roughly the mean free path of the particles [26]. The timestep is taken to be less than the relaxation of time. Collisions are then conducted within each cell according to the properties of the particles contained within it. Various collision models can be used, such as the hard sphere [24], variable hard sphere [27], variable soft sphere [28], and the generalized hard sphere model [29]. This study uses the variable soft sphere (VSS) model by Koura and Matsumoto [28] that modifies the simple hard sphere model by a temperature-dependent viscosity term (ω) and an angular scattering term (α). ω modifies the diameters of a particle as a function of the temperature as,

$$d_{eff} = d_0 \left(\frac{T}{T_{ref}}\right)^{\omega} \tag{2}$$

where, T_{ref} and d_0 are the reference temperature and diameter. α modifies the scattering angle by

$$\chi = 2\cos^{-1}\left(\frac{b}{d}\right)^{1/\alpha} \tag{3}$$

The VSS model parameters for the gases in this study are listed in Table I.

Gas	Molecular Mass ($\times 10^{-26}$kg)	d_eff ($\times 10^{-9}$nm)	ω	T_{ref}	α
Nitrogen	4.6495	0.3875	0.686	353.15	1.365
Helium	0.6642	2.2980	0.712	350	1.429

TABLE I
COLLISION PROPERTIES OF THE AIR BEARING FROM REF. [30]

Gas	Molecular Mass ($\times 10^{-26}$kg)	d_eff ($\times 10^{-9}$nm)	ω	T_{ref}	α
Nitrogen	4.6495	0.3875	0.686	353.15	1.365
Helium	0.6642	2.2980	0.712	350	1.429

TABLE II
COLLISION PROPERTIES OF THE AIR BEARING.

The DSMC method has been used to test the MGL theory on gas bearings in HAMR head-disk interfaces [31, 32]. The bearing force predicted by MGL and DSMC was with 4% of each other [14]. The DSMC method was initially developed for rarefied flows, so the particles are considered point masses [33]. However, in dense gases, such as that in the gas bearings of hard disk drives, the particles' inter-atomic forces and finite sizes can influence their behavior [34]. The consistent Boltzmann algorithm (CBA) was developed to account for the finite volume of the particles [35]. The first effect to consider the the increased collisions as the effective space available for particles to move freely is reduced. The Y-factor increased the collisions, given by [36],

$$Y = \frac{1 + 0.0555678 b_2 n + 0.013944551 b_2^2 n^2 - 0.0013396 b_2^3 n^3}{1 - 0.56943218 b_2 + 0.08289011 b_2^2 n^2} \tag{4}$$

where $b_2 = \frac{2}{3}\pi\sigma^3$, σ is the collision diameter and n is the number density. The second effect is the increase in the deflection of particles after collisions. This is illustrated in Fig. 2. On the left side (Fig. 2a), we track the trajectory of two particles (red dots) separated by a distance x and moving towards each other with speed v. As these particles are assumed to be point particles, at $t = x/2v$, the particles collide and change the direction of travel. Then, at $t = x/v$, they return to their initial positions, which are x units away. Then, Fig. 2b shows the collision of the same particles but with a diameter, d. Since they possess a finite diameter, the center-to-center distance between the two particles is equal to d at impact. Therefore, the collision occurs at $t = \frac{x-d}{2v}$. Then, after the collision, they retrace their path. However, at $t = x/v$, the final positions are separated by a distance d from their initial position. This extra displacement needs to be accounted for by Eq 5

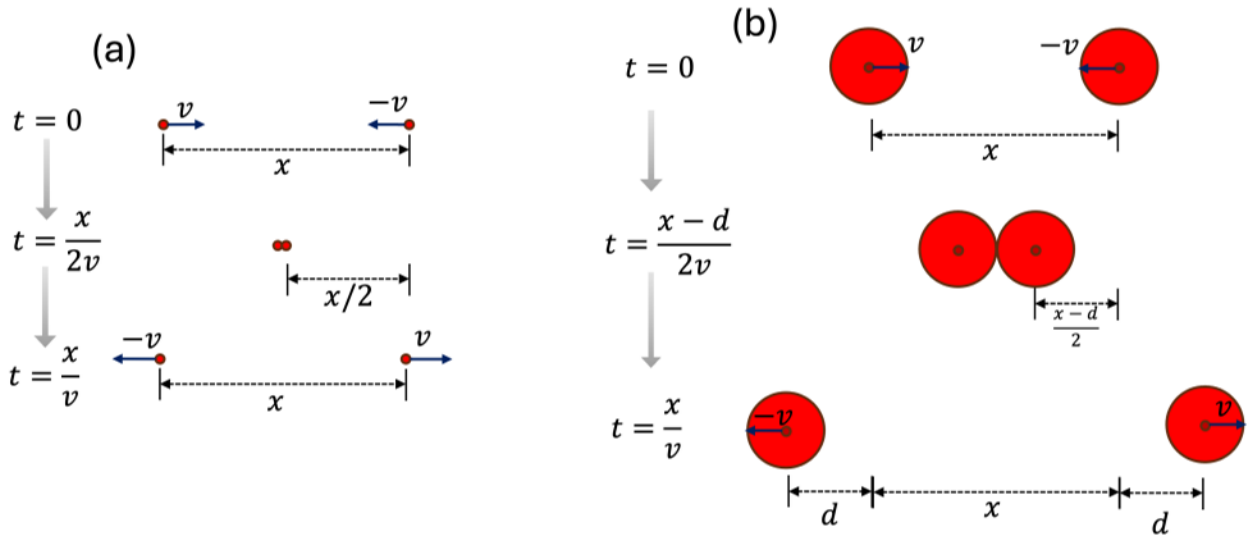

Fig. 2. Schematic to illustrate the need for CBA. (a) is the case when the particles are point masses. (b) is the case when the particles have a finite volume

$$\boldsymbol{d}_{cba} = \frac{\boldsymbol{v}_r' - \boldsymbol{v}_r}{|\boldsymbol{v}_r' - \boldsymbol{v}_r|}\sigma \tag{5}$$

where v_r and v_r' are the particles' pre and post-collision relative velocities. We ignore the inter-atomic forces in the study. When replicating the simulation conditions from Huang (1997) [14], we observe a 2% higher bearing force after applying CBA. Therefore this effect may be one source for the slight difference between the MGL and traditional DSMC model.

The DSMC method has been proven to converge to the Boltzmann equation [37], has been thoroughly tested in high Knudsen-number flows [25], and excellent agreement has been found with experiments [38]. Due to the relative simplicity of setting up a DSMC simulation, the ability to study gas mixtures, and the ability to couple optical fields, we use the modified DSMC to study the air-bearing. We use the open-source software SPARTA [39] to run all DSMC simulations in this study.

B. Simulation conditions

A typical hard drive slider is hundreds of microns in size, with special etchings on the air-bearing surface to produce the precise bearing force required to counter the head suspension load. The ABS designs used in HAMR drives are not public. Moreover, modeling such a large system would be computationally expensive in terms of computing power and memory requirements. Therefore, we use a simplified model that can capture the necessary characteristics of the HAMR head-disk interface. As shown in Fig 3, a channel with varying cross-sections is used. The top surface represents the head and has a peak temperature of 500 K. The bottom surface represents the disk with a peak temperature of 800 K. Further, it moves at a constant velocity of 50 m/s. Both surfaces behave like solid walls that reflect or reset the incident particle's velocity with a given accommodating factor, α. The velocity reset occurs according to a Maxwellian velocity distribution. Along the down-track direction is an inflow and outflow boundary condition with particles inserted or removed to maintain atmospheric pressure. The cross-section is designed to allow for smooth airflow near the inlet boundary. The channel dimensions are 15 μm in the down-track direction and 50 nm in the vertical direction. The channel width (into the plane) is assumed to be infinite, with period boundary conditions being enforced.

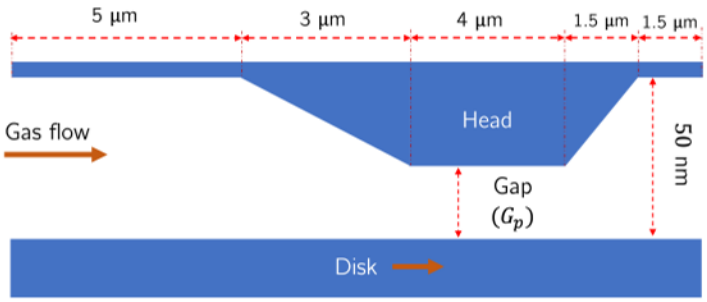

Fig. 3. Schematic view of the head-disk interface

The dimension of a DSMC cell must be less than the mean free path of the gas particles to consider particle collision pairs to be chosen that can actually collide. However, very small and uniform cell sizes would increase the computational costs. Since the mean free path depends on the temperature and pressure, we adapt the cell size to the local temperature and pressure. The maximum cell size was set to be 25 nm and the smallest to be 1 nm. The chosen timestep should also be smaller than the mean collision time. From kinetic theory, the mean collision time stood between 29 to 41 ps (picosecond) for the temperature and pressure ranges we countered. Thus, we used a conservative timestep of 10 ps for the rest of the simulation. We also allowed each simulation to reach equilibrium by waiting for about 150,000 steps before any measurements were made.

To simulate humidity, water vapor molecules were considered to be a separate gas. Each water molecule was approximated as a hard sphere with an effective diameter of 270 pm. The inlet and outlet boundaries were set at 20 % relative humidity ($\approx$ 700 Pa) pressure. As the temperature on the disk (800 K) exceeds the critical temperature of water, condensation would not occur on the disk surface. On the head surface (at 500 K), the water saturation pressure is around 25 bars, much greater than the expected partial pressure of water vapor, leading to negligible condensation. Therefore, condensation on the head surface could be ignored.

III. Results

We simulated a range of gaps from 2 nm to 25 nm for nitrogen and helium bearings. The top and bottom surfaces were divided into 2000 surface elements, and the pressure in each element was calculated by summing over the momentum change

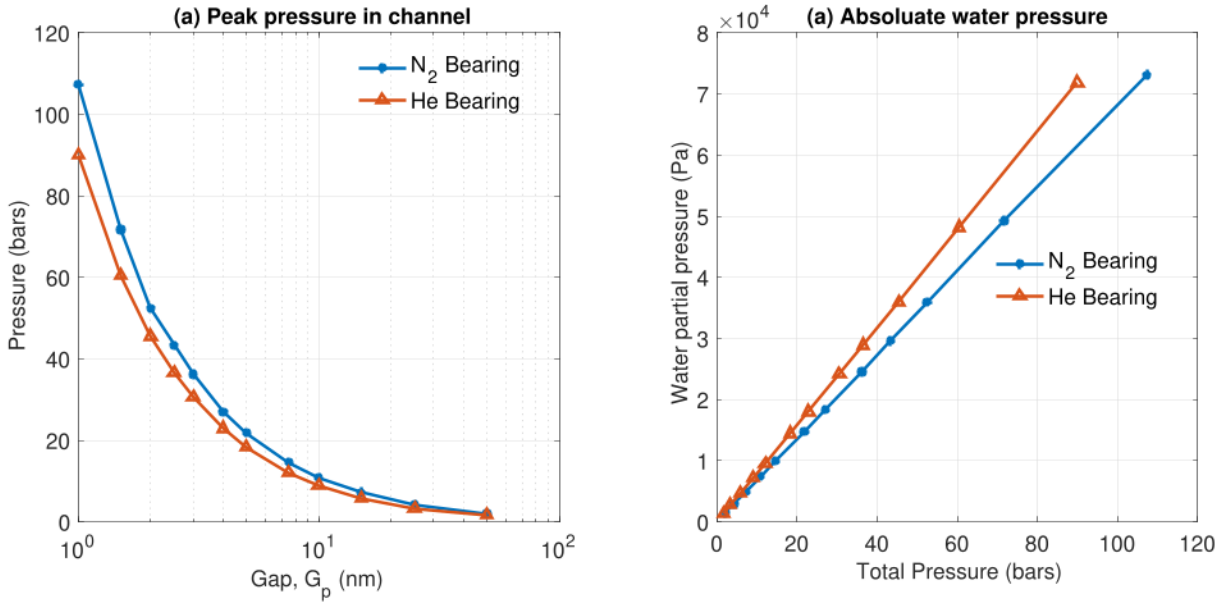

Fig. 4. (a) Peak pressure in the channel with hotspot, (b) Partial pressure of water at various total pressures

of incident molecules per unit time. The pressure over 400,000 timesteps were averaged to obtain uniform results. The pressure vs. spacing graph is plotted in Fig. 4a. As we would expect, the total pressure increases as the gap reduces. Nitrogen bearings showed a higher peak pressure due to its larger size and mass. Further, as seen in Fig. 4b, the pressure increase is also accompanied by a corresponding increase in the partial pressure of water. The absolute pressure reaches upwards of 40 kPa. This is feasible due to the high surface temperatures increasing the saturation pressure of water.

To investigate further, we plot the total pressure distribution at the top and bottom surfaces in Fig. 5. We observe that the pressure distributions on both surfaces are identical for helium and nitrogen. This must happen as any pressure gradient would lead to a net flux of particles to reach equilibrium. However, since the temperatures at the two surfaces differ by 300 K, the composition of the bearing at the two ends must be different to maintain equal pressure. The pressure depends on four quantities - the particle's mass, the number density, the temperature, and the correction term to account for non-ideal effects. In our case, the correction term is the diameter of the particle (Eq. 5). Since the particle's properties are constant throughout each simulation, the gas temperature and number density are the only variation that accounts for the constant pressure. At the particle level, the temperature and number density make sense only in a non-zero volume rather than at a surface or a point. Therefore, we calculate these quantities at the grid cell adjacent to each surface element. The adaptive grid cell size algorithm ensures that the dimension of the cell does not exceed the mean free path of a gas particle. Fig. 6 plots nitrogen bearings' number density and temperature distribution at 4 nm spacing. The solid lines mark the quantity along the bottom surface, and the dashed lines mark the quantity along the top surface. They show that the temperature and number density profiles follow different distributions at the top and bottom surfaces around the hotspot. This ensures that the pressure is equal even if the surface temperatures differ. In Fig. 7a, we plot the difference in number density at the top and bottom surface over a range of gaps. It shows that as the gap decreases, the difference increases between the two ends increases. As particles bounce off the surface, the diffusive boundary condition at the surfaces ensures that the kinetic energy of the particles corresponds to the surface temperature. Consequently, the particles bouncing off the hotter side have an average higher velocity than those from the cooler side. We can observe this in Fig. 8, where we plot the vertical component of the velocity along the down-track direction. As the particles traveling from the hotter to the colder surface have a larger mean speed than those traveling from the colder to the hotter surface, the gas flow has a non-zero vertical drift, which ensures that the number density at the colder end remains the same. As the gap reduces, the absolute number density also increases, leading to an increase in number density jump between the ends.

Further, Fig. 7b shows the temperature difference between the two sides. We observe a consistently small < 40 Kelvin temperature difference between the two ends, with the gas temperature at the bottom being the higher. This contrasts the difference in the top and bottom surface temperatures of 800 K and 500 K, respectively. This is because the gap limits the mean free path of the particles. For example, at 600 K, the mean free path of helium gas at 40 bars pressure is around 9 nm, lower than the corresponding gap of 2 nm. As a result, many particles have a direct trajectory between the surface. Hence, the velocity distribution of the molecules is defined by the ratio of particles that come from the top and bottom surfaces. Since the trajectory of the particles is near collision less, this ratio does not vary significantly along the vertical direction. This results in the temperature being approximately the average of the top and bottom surfaces.

In the simulated head-disk interface, the size of the temperature spot spans several hundred nanometers. In HAMR heads, the temperature spot would be in the tens of nanometers. This difference was necessary to allow the DSMC to yield good statistical averages. However, the smaller hotspots in HAMR heads may change in how fast the various fields reach equilibrium with the temperature fields on the head and disk surfaces.

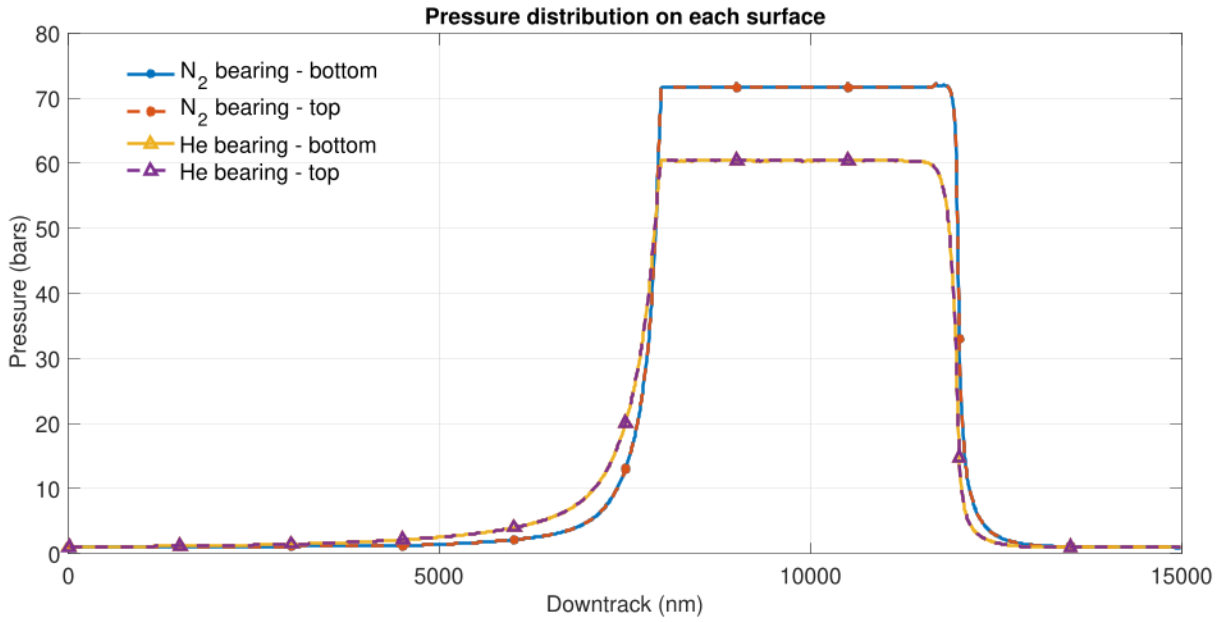

Fig. 5. Pressure distribution along the top and bottom surface for helium and nitrogen bearings at 4 nm gap

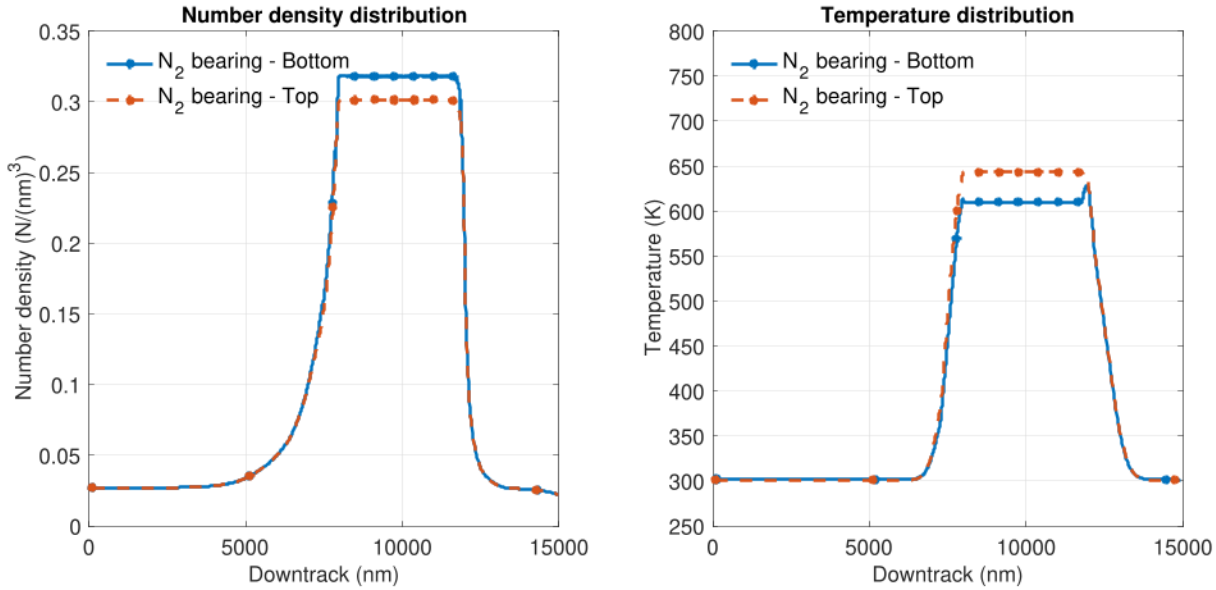

Fig. 6. (a) Number density distribution along the top and bottom surface for nitrogen-bearing with 4 nm gap (b) Temperature distribution along the top and bottom surface for nitrogen-bearing with 4 nm gap

If we now consider collisions in the gap, we see the collisionless trajectory clearly. Consider the two kinds of collision. The intermolecular collisions occur between the gas molecules and the surface collisions between the gas molecules and surfaces. We count the average of the collisions at various spacings at each timestep and plot in Fig. 9. The intermolecular collisions decrease with clearance as the pressure drop dominates. The surface collisions also decrease with spacing as the pressure exerted by the air-bearing reduces, causing fewer particles to hit each surface. We define the collision ratio as the number of surface collisions for every intermolecular collision. This ratio behavior at very low spacings (for the spacing we considered. The ratio is greater than 1, indicating that each gas particle collides with other particles after several surface collisions. This suggests that they follow a free molecular flow (collisionless trajectory) in these spacings, and the head disk clearance limits the mean free path. In other words, this regime resembles rarefied gas dynamics. Helium and nitrogen exhibit different ratios

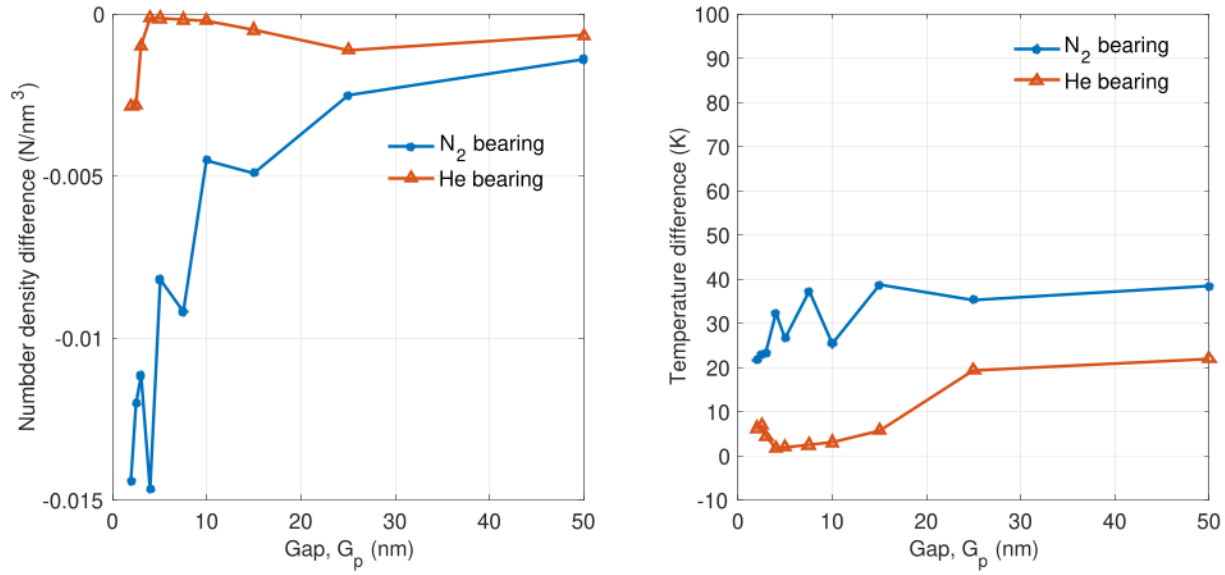

Fig. 7. (a) The average difference in the number density for gas bearings at different gap values (b) The average temperature difference for gas bearings at different gap values

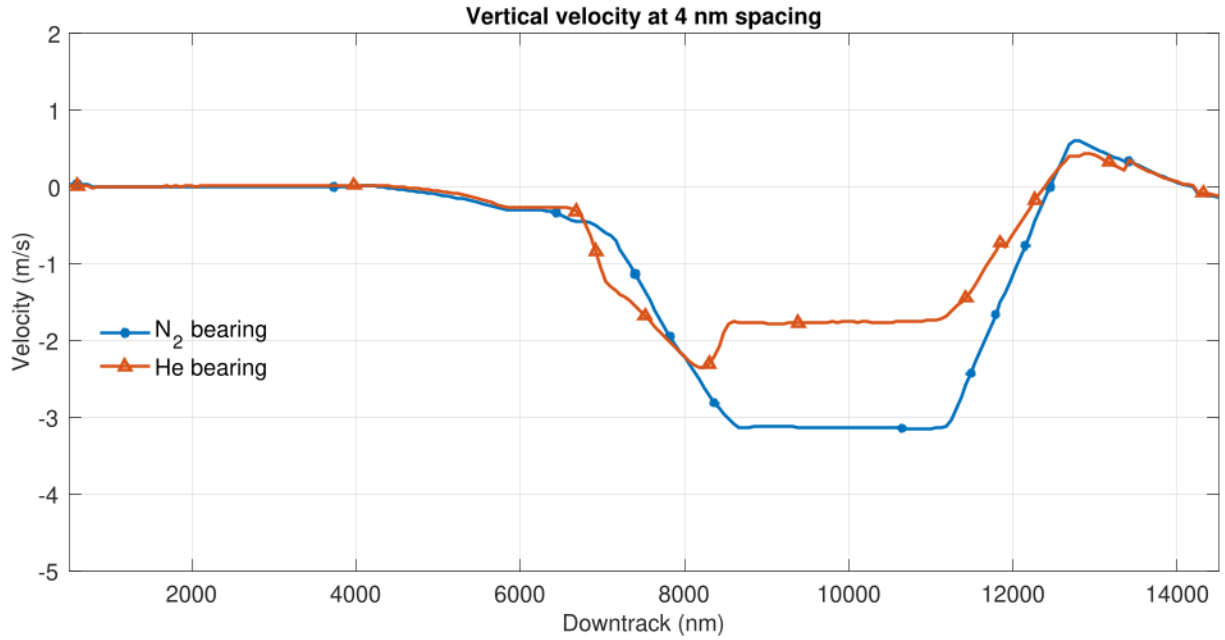

Fig. 8. The vertical component of the gas velocity for nitrogen and helium bearings at 4 nm gap

due to their molecule's sizes and mass. The faster helium atoms collide with the surface at a faster rate than the slower nitrogen molecules. The free molecular flow has several implications for the reliability of air-bearing, especially in the nature of the heat transfer mechanism [9], which may be enhanced due to the collisionless flow of particles. Further, it suggests that smear nanoparticles may travel unhindered by the moving gas in the head-disk spacings of HAMR drives.

IV. Conclusion

In this study, we used the DSMC method to study the gas bearings of hard disk drives. We first modified DSMC using the consistent Boltzmann algorithm to account for the dense gas effects. The stable nature of the DSMC method provides a convenient method to simulate the head-disk interface without worrying about numerical errors and instabilities. The results are summarized below:

1) The density and temperature fields do not significantly vary along the vertical direction. The temperature is approximately the average of the head and disk surfaces.
2) There is a non-zero vertical velocity component to maintain equal pressure on the head and disk surfaces.

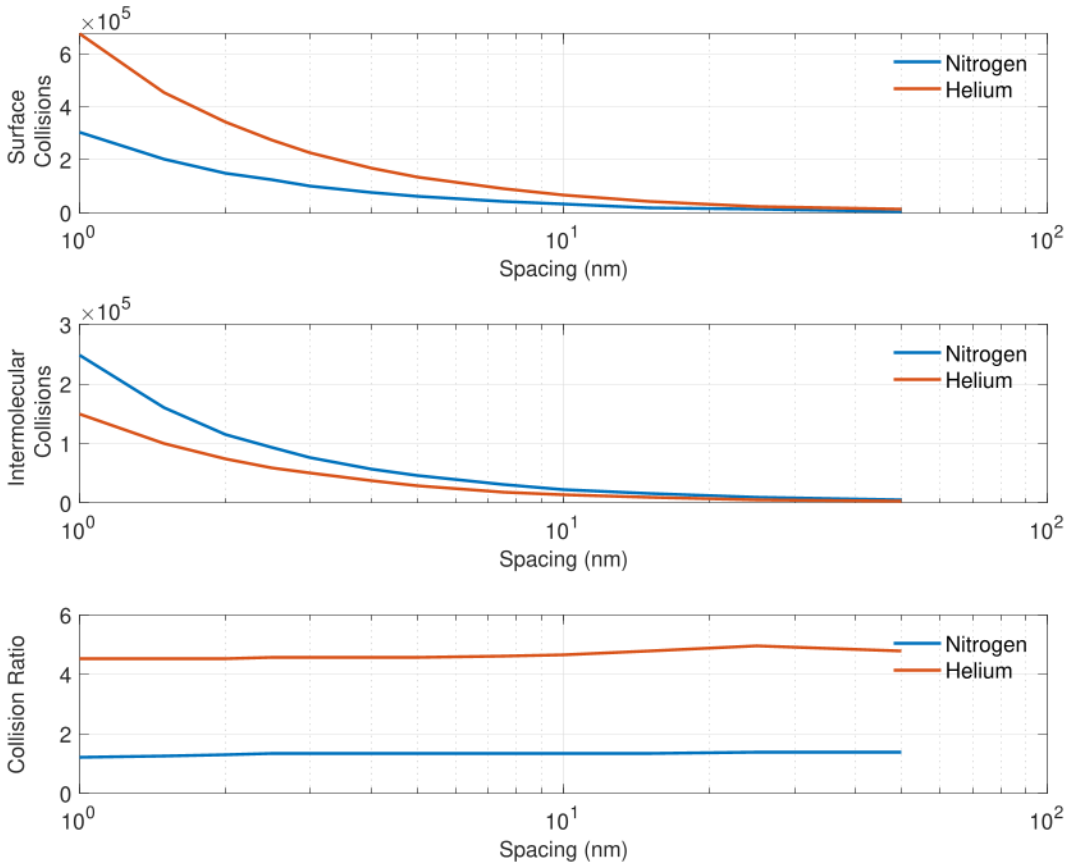

Fig. 9. (a) The surface collisions per timestep. (b) The intermolecular collisions per timestep. (c) The collision ratio (defined as the ration between the surface and intermolecular collisions)

3) The gas molecules largely undergo a free molecular path between the head and disk surfaces.
4) The high temperature allows water vapor concentration to increase with the air-bearing pressure.

This method can now be used to simulate smear transport if we assume that smear behaves like a granular gas [40]. However, a Lennard-Jones interaction model of Ref. [41], must be used to account for the intermolecular forces between the smear gas particles. Then, an appropriate adsorption mechanism [42] can then be used to record the smear growth on the head or disk surface. Further, the influence of other forces, for example, the optical force [4] on the smear gas, can be easily coupled into the simulation as an external field. The advection step modification of Eq 5 would then be further modified to include the acceleration due to the force field.

Acknowledgment

We thank Prof. Alejandro Garcia of San Jose State University for helpful discussions. This work was supported by the Computer Mechanics Lab at UC Berkeley.

References

[1] Steven Granz et al. “Heat Assisted Magnetic Recording Areal Density Dependence on Writer Current for Conventional and Shingled Magnetic Recording”. In: *2023 IEEE 34th Magnetic Recording Conference (TMRC)*. IEEE. 2023, pp. 1–2.
[2] Qilong Cheng and David B Bogy. “Experimental study of smear formation and removal in heat-assisted magnetic recording”. In: *Tribology International* 165 (2022), p. 107258.
[3] Shaomin Xiong et al. “Material Transfer From Media to Head in Heat Assisted Magnetic Recording (HAMR)”. In: *Information Storage and Processing Systems*. Vol. 84799. American Society of Mechanical Engineers. 2021, V001T05A003.
[4] Roshan Mathew Tom et al. “Optical forces in heat-assisted magnetic recording head-disk interface”. In: *Scientific Reports* 13.1 (2023), p. 8451.
[5] Roshan Mathew Tom, Qilong Cheng, and David B Bogy. “A Numerical Simulation of PFPE Lubricant Kinetics in HAMR Air Bearing”. In: *Tribology Letters* 72.2 (2024), pp. 1–11.
[6] Hiroshi Tani et al. “Effect of Humidity on Head Smear Generation in Head-Assisted Magnetic Recording”. In: *IEEE Transactions on Magnetics* 59.11 (2023), pp. 1–5.

[7] Xingyu Chen et al. “Effect of water on mechano-chemical reactions of perfluoropolyether lubricant films in heat-assisted magnetic recording: A reactive molecular dynamics study”. In: *Tribology International* 187 (2023), p. 108674.

[8] Kyosuke Ono. “Physics of the Sub-Monolayer Lubricant in the Head-Disk Interface”. In: *Lubricants* 12.4 (2024), p. 117.

[9] S Sakhalkar et al. “Numerical and experimental investigation of heat transfer across a nanoscale gap between a magnetic recording head and various media”. In: *Applied Physics Letters* 115.22 (2019).

[10] Hiroshi Tani et al. “Investigation of mechanism of smear formation from diamond-like carbon films on heating”. In: *Microsystem Technologies* 27 (2021), pp. 2243–2255.

[11] Qingkang Liu et al. “Study on the thermal decomposition of d-4oh PFPE lubricant by reactive molecular dynamic simulation for HAMR”. In: *IEEE Transactions on Magnetics* 59.3 (2022), pp. 1–7.

[12] Siddhesh V Sakhalkar and David B Bogy. “A model for lubricant transfer from media to head during heat-assisted magnetic recording (HAMR) writing”. In: *Tribology Letters* 65 (2017), pp. 1–15.

[13] S. Fukui and R. Kaneko. “Analysis of Ultra-Thin Gas Film Lubrication Based on Linearized Boltzmann Equation: First Report—Derivation of a Generalized Lubrication Equation Including Thermal Creep Flow”. In: *Journal of Tribology* 110.2 (Apr. 1988), pp. 253–261. ISSN: 1528-8897.

[14] Weidong Huang, David B Bogy, and Alejandro L Garcia. “Three-dimensional direct simulation Monte Carlo method for slider air bearings”. In: *Physics of Fluids* 9.6 (1997), pp. 1764–1769.

[15] Qilong Cheng, Yuan Ma, and David Bogy. “Effect of Humidity on the Nanoscale Heat Transfer at the Head-Media Interface”. In: *ASME 2019 28th Conference on Information Storage and Processing Systems* (June 2019). DOI: 10.1115/isps2019-7449. URL: http://dx.doi.org/10.1115/ISPS2019-7449.

[16] Nisha Shukla et al. “Effect of Humidity on Lubricated Carbon Overcoats”. In: *Tribology Letters* 12.2 (2002), pp. 105–109. DOI: 10.1023/a:1014085517456. URL: https://doi.org/10.1023/A:1014085517456.

[17] Dae-Young Lee et al. “Effect of relative humidity and disk acceleration on tribocharge build-up at a slider–disk interface”. In: *Tribology International* 40.8 (Aug. 2007), pp. 1253–1257. DOI: 10.1016/j.triboint.2006.11.006. URL: https://doi.org/10.1016/j.triboint.2006.11.006.

[18] Sang Hoon Kim et al. “Humidity effects on lubricant transfer in the head-disk interface of a hard disk drive”. In: *Journal of Applied Physics* 105.7 (2009). DOI: 10.1063/1.3061704.

[19] Qilong Cheng et al. “Dependence of nanoscale heat transfer across a closing gap on the substrate material and ambient humidity”. In: *Applied Physics Letters* 116.21 (May 2020). DOI: 10.1063/5.0010286. URL: https://doi.org/10.1063/5.0010286.

[20] Thomas E. Karis. “Water Adsorption on Thin Film Media”. In: *Journal of Colloid and Interface Science* 225.1 (May 2000), pp. 196–203. DOI: 10.1006/jcis.2000.6745. URL: https://doi.org/10.1006/jcis.2000.6745.

[21] Ryan Z. Lei and Andrew J. Gellman. “Humidity Effects on PFPE Lubricant Bonding to a-CHx Overcoats”. In: *Langmuir* 16.16 (July 2000), pp. 6628–6635. DOI: 10.1021/la9915973. URL: https://doi.org/10.1021/la9915973.

[22] G. W. Tyndall, R. J. Waltman, and J. Pacansky. “Effect of adsorbed water on perfluoropolyether-lubricated magnetic recording disks”. In: *Journal of Applied Physics* 90.12 (Dec. 2001), pp. 6287–6296. DOI: 10.1063/1.1413946. URL: https://doi.org/10.1063/1.1413946.

[23] R. R. Dubin et al. “Degradation of Co-based thin-film recording materials in selected corrosive environments”. In: *Journal of Applied Physics* 53.3 (Mar. 1982), pp. 2579–2581. DOI: 10.1063/1.330913. URL: https://doi.org/10.1063/1.330913.

[24] G A Bird. *Molecular gas dynamics and the direct simulation of gas flows*. en. Oxford Engineering Science Series. Oxford, England: Clarendon Press, May 1994.

[25] Francis J Alexander, Alejandro L Garcia, et al. “The direct simulation Monte Carlo method”. In: *Computers in Physics* 11.6 (1997), p. 588.

[26] GJ LeBeau. “A parallel implementation of the direct simulation Monte Carlo method”. In: *Computer methods in applied mechanics and engineering* 174.3-4 (1999), pp. 319–337.

[27] Kenichi Nanbu. “Variable hard-sphere model for gas mixture”. In: *Journal of the Physical Society of Japan* 59.12 (1990), pp. 4331–4333.

[28] Katsuhisa Koura and Hiroaki Matsumoto. “Variable soft sphere molecular model for inverse-power-law or Lennard-Jones potential”. In: *Physics of fluids A: fluid dynamics* 3.10 (1991), pp. 2459–2465.

[29] HA Hassan and David B Hash. “A generalized hard-sphere model for Monte Carlo simulation”. In: *Physics of Fluids A: Fluid Dynamics* 5.3 (1993), pp. 738–744.

[30] Andrew B. Weaver and Alina A. Alexeenko. “Revised Variable Soft Sphere and Lennard-Jones Model Parameters for Eight Common Gases up to 2200 K”. In: *Journal of Physical and Chemical Reference Data* 44.2 (June 2015). ISSN: 1529-7845. DOI: 10.1063/1.4921245. URL: http://dx.doi.org/10.1063/1.4921245.

[31] Francis J Alexander, Alejandro L Garcia, and Berni J Alder. “Direct simulation Monte Carlo for thin-film bearings”. In: *Physics of Fluids* 6.12 (1994), pp. 3854–3860.

[32] Shigehisa Fukui and Kiyomi Yamane. “DSMC/MGL comparisons of stresses on slider air bearing with nanometer spacings”. In: *IEEE transactions on magnetics* 38.5 (2002), pp. 2153–2155.

[33] Alejandro L Garcia and Wolfgang Wagner. “The limiting kinetic equation of the consistent Boltzmann algorithm for dense gases”. In: *Journal of Statistical Physics* 101 (2000), pp. 1065–1086.

[34] Johannes Diderik Van der Waals. *Over de Continuiteit van den Gas-en Vloeistoftoestand*. Vol. 1. Sijthoff, 1873.

[35] Francis J Alexander, Alejandro L Garcia, and Berni J Alder. “A consistent Boltzmann algorithm”. In: *Physical Review Letters* 74.26 (1995), p. 5212.

[36] JJ Brey et al. *25 Years of Non-Equilibrium Statistical Mechanics*. Springer, 1995.

[37] Wolfgang Wagner. “A convergence proof for Bird’s direct simulation Monte Carlo method for the Boltzmann equation”. In: *Journal of Statistical Physics* 66 (1992), pp. 1011–1044.

[38] E P Muntz. “Rarefied Gas Dynamics”. In: *Annual Review of Fluid Mechanics* 21.1 (Jan. 1989), pp. 387–422. ISSN: 1545-4479. DOI: 10.1146/annurev.fl.21.010189.002131. URL: http://dx.doi.org/10.1146/annurev.fl.21.010189.002131.

[39] Steve J Plimpton et al. “Direct simulation Monte Carlo on petaflop supercomputers and beyond”. In: *Physics of Fluids* 31.8 (2019). URL: http://sparta.sandia.gov.

[40] Nikolai V. Brilliantov and Thorsten Pöschel. *Kinetic Theory of Granular Gases*. Oxford University Press, July 2004. ISBN: 9780198530381. DOI: 10.1093/acprof:oso/9780198530381.001.0001. URL: https://doi.org/10.1093/acprof:oso/9780198530381.001.0001.

[41] Ayyaswamy Venkattraman and Alina A Alexeenko. “Binary scattering model for Lennard-Jones potential: Transport coefficients and collision integrals for non-equilibrium gas flow simulations”. In: *Physics of Fluids* 24.2 (2012).

[42] Krishnan Swaminathan Gopalan and Kelly A. Stephani. “Development of a Detailed Surface Chemistry Framework in DSMC”. In: *2018 AIAA Aerospace Sciences Meeting*. American Institute of Aeronautics and Astronautics, Jan. 2018. DOI: 10.2514/6.2018-0494. URL: http://dx.doi.org/10.2514/6.2018-0494.